# Effect of delithiation on the dimer transition of the honeycomb-lattice ruthenate $Li_{2-x}RuO_3$

Marco-Polo Jimenez-Segura,[1,*] Atsutoshi Ikeda,[1] Simon A. J. Kimber,[2] Carlotta Giacobbe,[2]
Shingo Yonezawa,[1] and Yoshiteru Maeno[1]

[1]*Department of Physics, Graduate School of Science, Kyoto University, Kyoto 606-8502, Japan*

[2]*European Synchrotron Radiation Facility (ESRF), 6 rue Jules Horowitz, B.P. 220, 38043 Grenoble Cedex 9, France*

(Received 1 March 2016; revised manuscript received 6 July 2016; published 29 September 2016)

The honeycomb-lattice ruthenate $Li_2RuO_3$ is made heavily Li deficient by chemical oxidation by iodine. The delithiation induces a different phase $Li_{2-x}RuO_3$, the "D phase," with superlattice. For the first time we disclose the magnetic and structural properties of the D phase in the dimer-solid state. The low-temperature magnetic susceptibility and the bond lengths indicate a bonding configuration consisting of both $Ru^{4+}$-$Ru^{4+}$ and $Ru^{5+}$-$Ru^{5+}$ dimers.

DOI: 10.1103/PhysRevB.94.115163

## I. INTRODUCTION

Honeycomb-lattice iridates of the type $A_2IrO_3$ ($A$ = Li, Na) with effective angular momentum $J_{\text{eff}} = 1/2$ due to strong spin-orbit coupling have been under active experimental investigation [1,2], mainly because of their interesting properties associated with predicted topologically nontrivial states, including the Kitaev spin-liquid state [3,4]. What is more, topological superconductivity has been proposed based on the Kitaev-Heisenberg model, with spin $S = 1/2$ emerging with hole doping [5–8].

Another interesting compound with the honeycomb structure is $Li_2RuO_3$. One difference from $A_2IrO_3$ is that $Li_2RuO_3$ has nominally $S = 1$, as expected for the low-spin state of $Ru^{4+}$ ($4d^4$). Interestingly, $Li_2RuO_3$ exhibits dimerization of Ru-Ru ions at $T_d \approx 540$ K, accompanied by a sharp decrease in magnetization below $T_d$ [9]. More recently, it was found that disorder in the Ru-Ru dimer configuration sensitively affects the magnetic behavior [10]. In addition, the dimer transition has been revealed to be of the first-order type [11], especially in samples with a more coherent dimer configuration with $T_d \approx 550$ K [10].

It has also been demonstrated that the dimer transition is not an ordinary Peierls transition. In a recent study based on a combination of high-energy x-ray diffraction (XRD), pair distribution function (PDF) analysis, and density functional theory (DFT) calculations, it has been found that the dimers dynamically survive even above $T_d$ [12]. Thus, the transition can be regarded as the change from a static "dimer-solid" state at low temperatures to a dynamic "dimer-liquid" state above $T_d$ [12].

To gain new insight into $Li_2RuO_3$, we focus on removing Li from this compound. The effect of Li deficiency on the dimer transition is of primary interest for the following reasons. First, hole doping by delithiation could lead to the spin $S = 1/2$ state and thus to various topological phases including exotic superconductivity. Second, the dimer formation may be substantially changed by Li deficiency or hole doping, leading to a possible new dimer state related to dimer-solid and dimer-liquid states.

Actually, the delitiation of $Li_2RuO_3$ has been studied for its potential utility as a material for batteries [13]. The delithiated series $Li_{2-x}RuO_3$ has been synthesized from $Li_2RuO_3$ by electrochemical deintercalation of lithium [14–16] and by chemical oxidation by $I_2$ [17]. Moreover, it has been revealed that a part of $Ru^{4+}$ changes to $Ru^{5+}$ by delithiation based on a sequence of experiments [18–20]. However, concerning the physical properties of $Li_{2-x}RuO_3$, only magnetization has been reported in the limited temperature range between 83 and 293 K [17]. In particular, the relation between the dimer transition and delithiation has not been reported.

In this work, we report properties of heavily delithiated $Li_{2-x}RuO_3$ obtained by chemical oxidation. We confirm a crystallographic phase distinct from the pristine phase. This phase, emerging by heavy delithiation, shall be called the "D phase." We compare structural and magnetic properties of the D phase with those of the stoichiometric "S phase." In particular, we find in the D phase a new dimer-solid state with an electronic configuration different from that in the S phase.

## II. EXPERIMENT

Pristine $Li_2RuO_3$ samples were prepared from $Li_2CO_3$ (Aldrich; 99.997%) and $RuO_2$ (Rare Metallic; 99.9%) by means of solid-state reaction. After the starting powders were dried, stoichiometric quantities were mixed and ground for 1 h in a conventional mortar. We added acetone to improve the homogeneity of the powder [10]. The powder was pelletized and heated at 1000°C for 24 h in the first step. Next, the pellet was reground in acetone for 1 h, pelletized, and heated at 900°C for 48 h, followed by natural cooling. This choice of the synthesis procedure is based on the previous study [10]. Purity, as well as coherence, of the dimer configuration was verified by XRD and magnetic susceptibility measurements as described below.

Delithiation was performed based on the reaction

$$Li_2RuO_3 + \frac{y}{2}I_2 \xrightarrow{CH_3CN} Li_{2-x}RuO_3 + xLiI + \frac{y-x}{2}I_2. \quad (1)$$

$I_2$ (Wako; 99.9%) was dissolved in acetonitrile ($CH_3CN$) at a concentration of 0.3384 mol/L. After precise measurement of its mass, the powder of $Li_2RuO_3$ was soaked in the iodine solution for 3 days at room temperature. Then the $Li_{2-x}RuO_3$ powder was washed with clean acetonitrile. Since XRD

*m.jimenez@fkf.mpg.de

 ©2016 American Physical Society

analysis indicated that stronger delithiation was necessary, after another measurement of the mass, the powder was soaked in a new solution of $I_2$ (0.3683 mol/L) for 18 h under stirring at 560 rpm. The containers were covered with aluminum foil in order to avoid the conversion of $I^-$ into $I_2$ triggered by light. The $Li_{2-x}RuO_3$ powder was taken out, then rinsed with clean acetonitrile until the acetonitrile became completely transparent. A less delithiated sample of $Li_{2-x}RuO_3$ was prepared in a solution of $I_2$ (0.18457 mol/L). In this case, a pellet of $Li_2RuO_3$ was soaked for 3 days. We stored samples in vacuum, although there is no noticeable decomposition at room temperature in air for either pristine or delithiated samples.

In order to evaluate the value of $x$, the remaining quantity of $I_2$ in acetonitrile was measured through titration [21,22] with a standard solution of $Na_2S_2O_3$ (Wako; 0.05 mol/L for volumetric analysis) at 19°C based on the reaction

$$I_2 + 2S_2O_3^{2-} \rightarrow 2I^- + S_4O_6^{2-}. \quad (2)$$

The glassware used for titration was calibrated at 19°C with acetonitrile. Completion of this reaction is monitored by the color of starch added to the solution. We find that the total lithium extracted is $x \approx 0.73$ and 0.34 for the two delithiated samples presented in this paper.

We also performed an inductively coupled plasma-optical emission spectroscopy (ICP-OES) analysis using a commercial apparatus (Seiko Instruments; SPS 6100). Quantitative evaluation of $x$ by ICP-OES was not successful because $Li_{2-x}RuO_3$ cannot be dissolved completely into standard acids (such as HCl), due to production of insoluble $RuO_2$ in the acid.

Laboratory XRD measurements were carried out with a commercial diffractometer (Bruker; D8 Advance) using Cu$K\alpha$ radiation ($\lambda = 1.54184$ Å, $E = 8.041$ keV) equipped with a one-dimensional array of detectors and a nickel monochromator. High-energy XRD measurements at room temperature were performed at beam line ID22 of the European Synchrotron Radiation Facility (ESRF). An x-ray beam of energy 30.993 keV ($\lambda = 0.4000$ Å) was used. High-energy XRD measurements at various elevated temperatures were performed at beam line ID11 at the ESRF. A double Laue monochromator was used to select an x-ray of energy 87.5 keV ($\lambda = 0.141$ Å). The beam was focused to ca. 100 mm using refractive lenses. The scattered x-ray was detected using a CCD camera (FReLoN). Temperature control was achieved using a hot-air blower. Data were continuously collected upon heating to 723 K at 2.5 K/min and upon cooling to room temperature at the same rate. Typical temperature resolution was 0.2 K/pattern. We find a noticeable difference between the actual sample temperature and the thermometer temperature. Thus, a lineal correction to the thermometer temperature was made, so that the $T_d$ of $Li_2RuO_3$ recorded in XRD measurements matches the $T_d$ in magnetization measurements.

Magnetization measurements were performed using a commercial superconducting quantum interference device magnetometer (Quantum Design; MPMS). Magnetization at high temperatures (300 to 700 K) was measured using the oven option for the MPMS. We used quartz tubes as sample holders for high-temperature measurements. Sample tubes were sealed with ceramic bond (Resbond; 907GF) in order to prevent any gas released from the sample from damaging the inside of the oven sample space. We checked the thermometer calibration of the oven by measuring the ferromagnetic transition ($T_C = 627.2$ K) of Ni (rare metallic; 99.99%) at several fields [23]. The calibration error in $T_C$ of Ni is less than 0.2%. Measurements from 1.8 to 300 K were performed with the ordinary setup of the MPMS in zero-field-cooled (ZFC) and field-cooled (FC) sequences.

## III. RESULTS AND DISCUSSION

### A. Structure

Figure 1 shows the high-energy powder XRD spectra for $Li_{2-x}RuO_3$ samples with various values of $x$ measured at room temperature. This provides high-resolution spectra containing clear superlattice peaks at low angles. Figure 2 shows Cu$K\alpha$ XRD with Rietveld fitting. The pristine ($x = 0$) sample exhibits the patterns expected for pure $Li_2RuO_3$. The spectrum can be well fitted with the space group (SG) $P2_1/m$ [No. 11; Fig. 2(a)] as reported previously [9–12,24].

The delithiated samples exhibit patterns with substantial differences compared with the $x = 0$ sample as described below. The $x \approx 0.73$ sample, exhibiting almost-single-phase behavior, has the ($h$00) and (00$l$) peaks shifted to lower angles and the (0$k$0) peaks shifted to higher angles [Fig. 1(c)], indicating an increase in the values of $a$ and $c$ and a decrease in

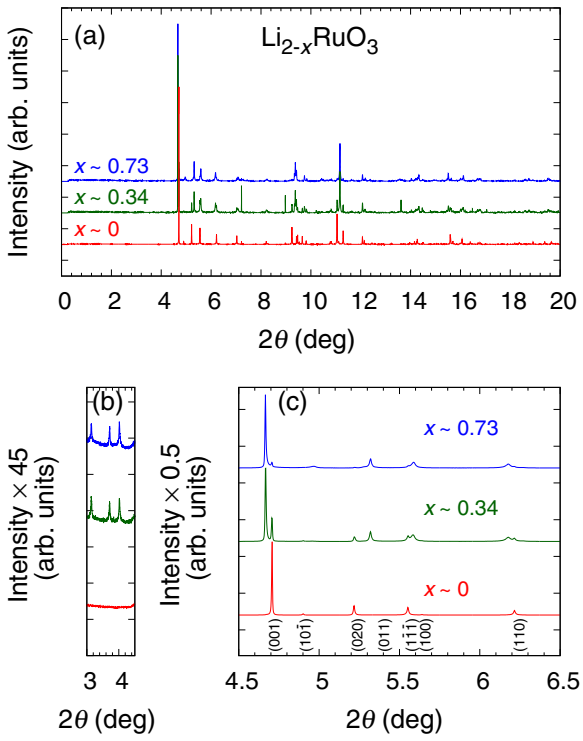


FIG. 1. Composition variations of the high-energy powder XRD spectra at room temperature of $Li_{2-x}RuO_3$ samples with $x = 0$, 0.34, and 0.73, taken with x rays of 30.993 keV ($\lambda = 0.4000$ Å) at beam line ID22 of the ESRF. Data in the ranges (a) $0° < 2\theta < 20°$, (b) $3° < 2\theta < 4.5°$, and (c) $4.5° < 2\theta < 6.5°$. The peak indices of the stoichiometric $Li_2RuO_3$ are shown in (c) based on the room-temperature crystal structure reported by Miura *et al.* [9]. The (10$\bar{1}$) peak is characteristic of the dimer-solid state [9,12].

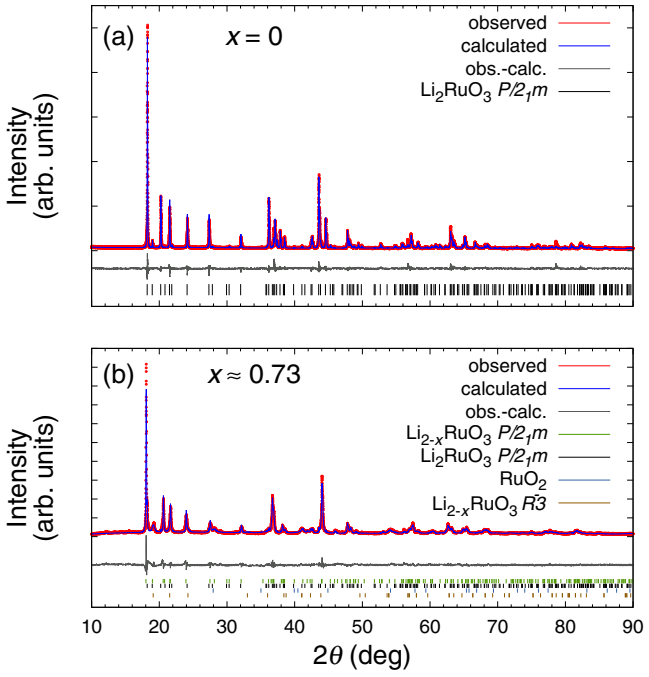


FIG. 2. Rietveld refinement of the Cu$K\alpha$ XRD ($\lambda = 1.54184$ Å, $E = 8.041$ keV) of samples of (a) $Li_2RuO_3$ with $x = 0$ and (b) $Li_{2-x}RuO_3$ with $x = 0.73$. In both cases SG $P2_1/m$ was used. Parameters of the fitting are listed in Table I. The structure factor used in both cases is that of $Ru^{4+}$ because the structure factors of $Ru^{5+}$ are not available in our software. The measurement time for $x = 0.73$ was approximately twice as long as that for $x = 0$.

the value of $b$. Nevertheless, the spectrum of this delithiathed sample can be well fitted also with the SG $P2_1/m$ [Fig. 2(b)]. We designate the crystallographic phase observed in the $x \approx 0.73$ sample the D phase. In addition to the main peaks associated with the D phase, we can identify minor phases such as the S phase $Li_2RuO_3$, $RuO_2$, and yet another delithiated phase, $Li_{2-x}RuO_3$, with $x \approx 1.1$ (SG $R\bar{3}$, No. 148) [14].

For the sample with $x \approx 0.34$, we find that the XRD peaks such as (001) and (020) are clearly split into two peaks [Fig. 1(c)]: one group similar to those of the $x = 0$ sample and the other similar to those of the $x \approx 0.73$ sample. This fact indicates that the crystal-structure change due to delithiation is not continuous: there are two crystallographically distinct phases with $x = 0$ and $x > 0$ and they coexist at a comparable ratio in the $x \approx 0.34$ sample. For this sample, we estimate the mass fraction of the D phase within the sample to be about 70% from the intensity ratio of the main x-ray peaks. In the following analysis of these phases, we use the data for single-phase samples with $x = 0$ and $x \approx 0.73$.

In addition to the shifts in the main peaks, three small but sharp peaks are observed in the delithiated samples at $2\theta = 3.140°$, $3.714°$, and $4.017°$ [$d = 7.30$, 6.18, and 5.71 Å, Fig. 1(b)], indicating the presence of a superlattice structure. Although these small peaks have not been reported in pristine or delithiated $Li_2RuO_3$, a superlattice in $Li_{2-x}Ru_{1-y}M_yO_3$ ($M$ = Mn, Sn) has recently been found as additional spots in electron diffraction [18,19]. In these studies, the structure has approximately been described with the SG $C2/m$ (neglecting

TABLE I. Cell parameters of $Li_2RuO_3$ (S phase) and $Li_{2-x}RuO_3$ ($x \approx 0.73$; D phase) at room temperature obtained from laboratory XRD spectra. The space group used for both phases is $P2_1/m$.

| $x$ | $a$ (Å) | $b$ (Å) | $c$ (Å) | $\beta$ (deg) | $\sqrt{3}a/b$ | $R_{wp}$ | $R_e$ | $\chi^2$ |
|---|---|---|---|---|---|---|---|---|
| 0 | 4.922 | 8.787 | 5.896 | 124.36 | 0.970 | 10.96 | 7.31 | 1.50 |
| 0.73 | 4.937 | 8.630 | 5.898 | 123.54 | 0.991 | 11.35 | 4.37 | 2.60 |

the presence of the superlattice and Ru-Ru dimers even for small values of $y$). It has been suggested that the origin of the superlattice is the distortion in the oxygen positions [18,20]. Another possibility is an ordering of Ru valency (charge order) as we discuss latter. Since the SG in $Li_{2-x}RuO_3$ with the superlattice taken into account is not trivial, we hereafter consider the SG $P2_1/m$ to evaluate the cell parameters and the Ru ion positions.

As discussed previously, the cell parameters of the S and D phases, obtained from the laboratory XRD data, are compared in Table I. The parameters $a$ and $b$ for $Li_{2-x}RuO_3$ are longer and shorter than those for $Li_2RuO_3$, respectively. Studies on $Li_2Ru_{1-y}Mn_yO_3$ revealed the same trend of change in $a$ and $b$ when lithium is deintercalated, although the structure of $Li_2Ru_{1-y}Mn_yO_3$ is described with the SG $C2/m$[19]. Furthermore, the ratio $\sqrt{3}a/b$ of $Li_{2-x}RuO_3$ is closer to unity than that of $Li_2RuO_3$ (Table I). Thus, on average, the structure of $Li_{2-x}RuO_3$ seems to be more symmetric. Figure 3 compares the difference in bond lengths between the S and D phases. Reflecting the dimer-solid state in the S phase, the dimer bond $L_2$ is ≈16% shorter than the long bonds $L_1$ and $L_3$. In contrast, for the D phase, the difference is only about 6%. In Sec. III C, we discuss local structures in more detail.

Figure 4 shows high-energy XRD patterns ($E = 87.5$ keV, $\lambda = 0.141$ Å) of the $x \approx 0.73$ sample (dominated by the D phase) at selected temperatures upon heating (302 to 694 K) and after subsequent cooling (333 K). While heating, the

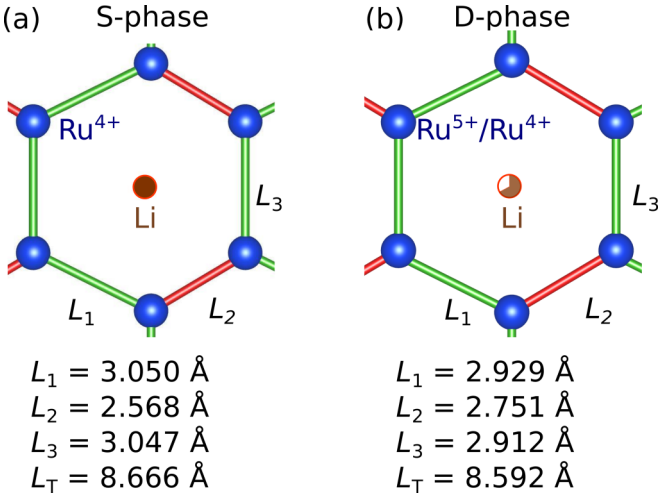


FIG. 3. Bond lengths $L_1$, $L_2$, and $L_3$ of the S phase and D phase. The sum of the bond lengths $L_T$ is given by $L_1 + L_2 + L_3$. Blue and brown spheres represent Ru and Li ions, respectively; red and green bars, short and long bonds. Figures were prepared with the program VESTA [25].

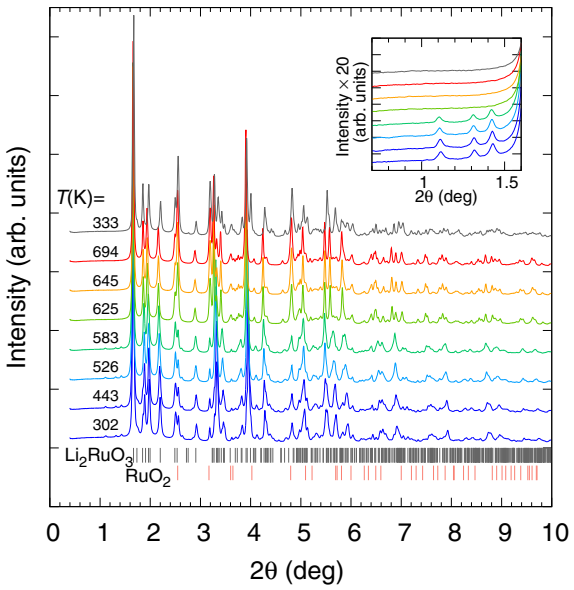


FIG. 4. Temperature variations of the high-energy XRD spectra for the $x \approx 0.73$ sample with $E = 87.5$ keV ($\lambda = 0.141$ Å) measured at beam line ID11 of the ESRF. Colors of the spectral curves correspond to the temperature region in the magnetization curve of the $x \approx 0.73$ sample in Fig. 5. Inset: Spectra in the range $0.7^\circ < 2\theta < 1.5^\circ$. Spectra for 302 to 664 K were obtained during the heating process, while the spectrum at 333 K was measured after cooling. Vertical lines at the bottom indicate the expected peak positions for $Li_2RuO_3$ and $RuO_2$.

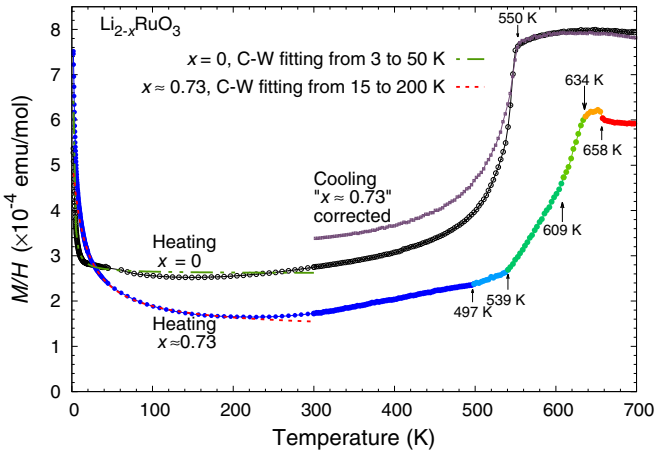


FIG. 5. Magnetic susceptibility vs temperature of the $x = 0$ sample (S phase) and the $x \approx 0.73$ sample (mostly D phase) from 1.8 to 700 K at $H = 10$ kOe. Corrections of diamagnetic contributions of ion cores have been made [27]. From 1.8 to 300 K, the magnetization was measured during warm up after ZFC. From 300 to 700 K the magnetization was measured in temperature upsweep, except for the purple curve, which is for the molar susceptibility of $Li_2RuO_3$ contained in the $x \approx 0.73$ sample upon cooling from 700 to 300 K (see text). Results of the Curie-Weiss fitting [$\chi = C/(T - \Theta) + \chi_0$] are also shown, by dashed curves. Colors of the curve for $x \approx 0.73$ correspond to those in Fig. 4.

three superlattice peaks between $2\theta = 1.1^\circ$ and $1.5^\circ$ disappear at ≈609 K. At the same temperature, a sudden increase in the $RuO_2$ peak intensity, for example, the one at $2\theta = 3.2^\circ$, is observed. These facts indicate the decomposition of $Li_{2-x}RuO_3$ ($x \approx 0.73$) into $Li_2RuO_3$ and $RuO_2$ starting at this temperature (see Appendix A for details).

Here we comment on differences in crystalline properties of delithiated $Li_{2-x}RuO_3$ and disordered $Li_2RuO_3$[10,26]. First, $Li_{2-x}RuO_3$ exhibits clearly distinct crystallographic phases, which are not reported for disordered $Li_2RuO_3$. Second, the superlattice structure observed in $Li_{2-x}RuO_3$ is absent in disordered $Li_2RuO_3$. In addition, the magnetic properties are also different between the two systems as we explain below. Therefore, $Li_{2-x}RuO_3$ is distinct from disordered $Li_2RuO_3$ and the observed behavior of the former cannot be solely ascribable to the disorder.

### B. Magnetization

Figure 5 shows the temperature dependence of the magnetic susceptibility of the $x = 0$ and $x \approx 0.73$ samples. Diamagnetic contributions of ion cores have been subtracted [27]. The overall shapes of curves for these samples differ in several aspects. At low temperatures, both samples exhibit Curie-like behavior; the difference will be discussed later. Both samples exhibit a minimum of magnetic susceptibility, but at different temperatures: ∼150 K for the sample with $x = 0$ and ∼200 K for the sample with $x \approx 0.73$. The susceptibility around this temperature range is smaller in the delithiated sample than in the pristine sample. This is in contrast to the disorder effect: in disordered $Li_2RuO_3$, the magnetic susceptibility around 100–200 K increases as the disorder increases [10]. Thus, the magnetic behavior in $Li_2RuO_3$ originates not from disorder, but from the electronic change due to Li deintercalation. With increasing temperature, the magnetic susceptibility of both samples increases toward the transition from dimer solid to dimer liquid. The change in the magnetic susceptibility in the pristine sample $Li_2RuO_3$ is relatively gradual below ∼500 K, followed by a sharp jump characteristic of the first-order transition (Appendix B). In contrast, the sample with $x \approx 0.73$ does not exhibit a gradual change below the transition but exhibits a clearer change in the slope of the $M(T)/H$ curve at $T \approx 539$ K. Between this temperature and 609 K, no clear change in the averaged crystalline structure was observed and the superlattice peaks are maintained (inset in Fig. 4). Thus, the change in the susceptibility seems to be mainly linked to changes in the electronic state, and not to chemical decomposition.

At 609 K, there is another change of slope in the $M(T)/H$ curve (Fig. 5). As already explained, the decomposition of $Li_{2-x}RuO_3$ into $Li_2RuO_3$ begins at this temperature (see also Appendix A). Therefore, the slope change at 609 K is mainly due to decomposition. Thus, in the warming run the susceptibility of the $x \approx 0.73$ sample above 609 K represents the sum of those of evolving multiple phases. During warming above 658 K, there is a slight but sharp drop in the susceptibility of the $x \approx 0.73$ sample (dominated by the S phase at this temperature). Across this temperature, there is no noticeable anomaly in the XRD spectra. Thus, the sharp drop probably

reflects a reorganization of lithium or oxygen induced by the vacancies of lithium in the initial $Li_{2-x}RuO_3$.

The purple curve in Fig. 5 is obtained from the susceptibility in the cooling process of the $x \approx 0.73$ sample after decomposition. Under this condition, the sample is dominated by $Li_2RuO_3$ and $RuO_2$ (see Appendix A). The raw data match the susceptibility shown by the red curve of the $x \approx 0.73$ sample above $T = 658$ K. The molar susceptibility of $Li_2RuO_3$ contained in the decomposed $x \approx 0.73$ sample was estimated using Eq. (A1) and the susceptibility of $RuO_2$ [28]. The result is shown by the purple curve in Fig. 5, which indeed matches that of pristine $Li_2RuO_3$ above ~550 K. However, the molar susceptibility shown by the purple curve at room temperature is ~18% larger than that of the pristine $x = 0$ sample. This is attributable to the less coherent dimer configuration in $Li_2RuO_3$ after decomposition of $Li_{2-x}RuO_3$ [10].

We performed a Curie-Weiss fitting to the susceptibility at low temperatures. The fitting temperature ranges (listed in Table II) are chosen so that the positive slope in $M(T)/H$ associated with the dimer transition at $T_d$ does not affect the fittings. Results of the fitting with the Curie-Weiss law $\chi(T) = \chi_0 + C/(T - \Theta)$ are shown by dashed curves in Fig. 5. From the fittings, we obtain the Curie constant ($C$) and the Weiss temperature ($\Theta$) as $C = 0.00039$ emu K/mol and $\Theta = 0.96$ K for the $x = 0$ sample and $C = 0.00625$ emu K/mol and $\Theta = -16$ K for the $x \approx 0.73$ sample. These results imply that the number of localized spins is rather small even for the $x \approx 0.73$ sample.

In an earlier study, it is proposed that samples with broad magnetic transitions at $T_d$ are accompanied by a dimer decoherent configuration, namely, dimer patterns breaking the long-range-ordered configuration [10]. Such a decoherent configuration results in nondimerized Ru ions with finite spin. To examine the number of such nondimerized ions, we assume that they exhibit $S = 1$ and $S = 3/2$ for the S phase and D phase, respectively, and that they can be treated as nearly free spins. From the Curie-Weiss fitting described above, the quantity of nondimerized ions is 0.039% for the $x = 0$ sample and 0.33% for the $x \approx 0.73$ sample. It is important to note that the obtained number of nondimerized ions in the $x \approx 0.73$ sample is much smaller than the number of vacancies of lithium or, equivalently, the number of $Ru^{5+}$ ions. This fact indicates that most of the Ru ions form dimers even in the D phase.

Figures 6(a) and 6(b) compare the low-temperature susceptibilities for the $x = 0$ and $x \approx 0.73$ samples. It is noticeable in Fig. 6(b) that the sample with $x \approx 0.73$ at low fields exhibits magnetic hysteresis below 12 K. Since the Weiss temperature $\Theta$ is negative, this hysteresis is probably due to magnetic ordering with antiferromagnetic interactions. No trace of superconductivity was found by ac susceptibility measurements using an adibatic demagnetization refrigerator [29] or transport measurements down to 0.1 K.

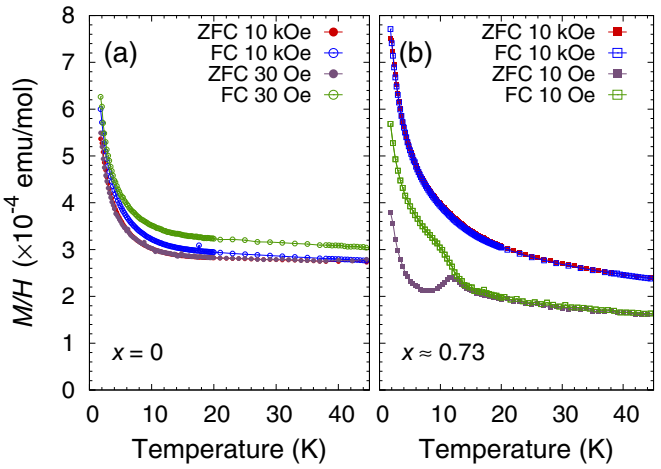


FIG. 6. Magnetic susceptibility vs temperature of (a) $Li_2RuO_3$ and (b) $Li_{2-x}RuO_3$ ($x \approx 0.73$) from 1.8 to 45 K at different magnetic fields measured in ZFC (filled symbols) and FC (open symbols) processes.

### C. Electronic configuration of dimers

According to the outcome described in the last section, the D phase is dominated by Ru-Ru dimers. In this section, we discuss the electronic configuration of these dimers and their correlation with the crystalline structure.

We first discuss the probable valency of Ru ions in the D phase. It has been demonstrated by x-ray photoemission spectroscopy, Mössbauer spectroscopy, electronic paramagnetic resonance measurements, and DFT calculations that the deintercalation of lithium from $Li_2RuO_3$ leads to the valence change from $Ru^{4+}$ to $Ru^{5+}$. In a higher $x$ range than $x = 1$, where Ru ions are fully oxidized to pentavalent, it is revealed that further delithiation induces loss of oxygen, appearance of peroxides ($O_2^{2-}$), and oxidation of $Ru^{5+}$ into $Ru^{6+}$ ions [18–20]. Based on those results, in the sample of $Li_{2-x}RuO_3$ with $x \approx 0.73$, the ratio of the amount of $Ru^{5+}$ among the total Ru ions would be similar to this $x$ value, and the others remain $Ru^{4+}$. In other words, the valency of the sample can be approximately expressed as $Li_{2-x}Ru^{4+}_{1-x}Ru^{5+}_xO_3$.

For the S phase, it is expected that magnetization is governed by the $Ru^{4+}$ ($4d^4$) ion. The origin of the decrease in magnetization below $T_d$ has been attributed to the formation of dimers with molecular orbitals (MOs) with $S \approx 0$ [30]. In contrast, the greater magnetization above $T_d$ has been explained by the partial breakdown of MOs. In the dimer-liquid state above $T_d$, Ru $4d$ orbitals keep the MO formed only by $\sigma$ bonds, leading to dynamic dimers [12].

Since the Curie-Weiss analysis indicates that most of the Ru ions form dimers with $S = 0$ even in $Li_{2-x}RuO_3$, there are three possible electronic configurations of the dimers in the

TABLE II. Curie-Weiss fitting parameters, expected Curie constants, and localized spins.

| $x$ | Curie constant. (emu K/mol) | $\Theta$(K) | $\chi_0$ (emu/mol) | $\mu_{\text{eff}}$ ($\mu_B$) | Fitting range (K) | Expected spin | Localized spins(%) |
|---|---|---|---|---|---|---|---|
| 0 | 0.00039 | 0.96 | 0.0002610 | 0.056 | 3–50 | 1 | 0.039 |
| 0.73 | 0.00625 | −16.0 | 0.0001349 | 0.22 | 15–200 | 3/2 | 0.333 |

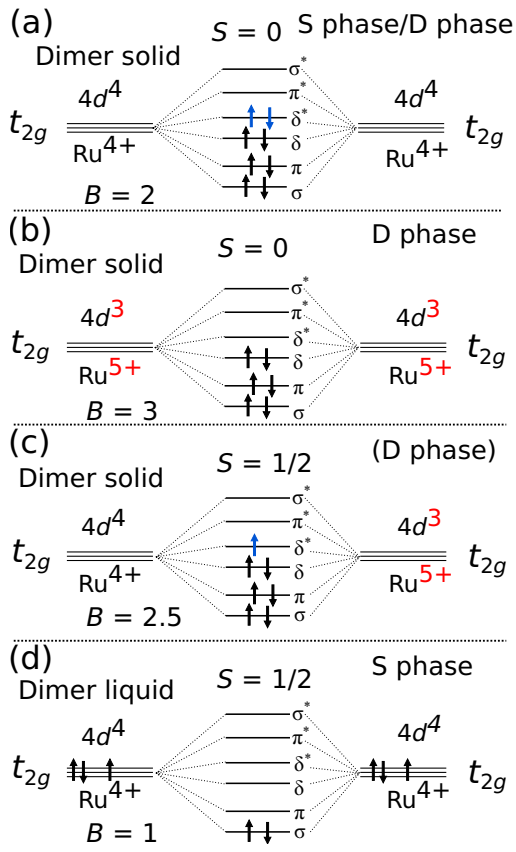


FIG. 7. Molecular orbital diagrams of possible configurations of the dimers of $Li_2RuO_3$ (S phase) and $Li_{2-x}RuO_3$ (D phase). Molecular orbitals in the dimer-solid state consisting of (a) $Ru^{4+}$-$Ru^{4+}$, (b) $Ru^{5+}$-$Ru^{5+}$, and (c) $Ru^{4+}$-$Ru^{5+}$ dimers, respectively. The configuration in (c) is less likely to occur based on the observed magnetic susceptibility. (d) Molecular orbitals in the dimer-liquid state formed by $Ru^{4+}$-$Ru^{4+}$ ions proposed in Ref. [12]. $B$ is the bond order defined by Eq. (3).

dimer-solid state as depicted in Fig. 7. The configuration in Fig. 7(a) was already proposed for the S phase [9,12,30].

We propose that in the D phase the most probable configuration for $Ru^{5+}$ is the dimer formed between $Ru^{5+}$ and $Ru^{5+}$ [Fig. 7(b)], since this dimer has electrons only in the lower-energy bonding states. In contrast, the dimers formed between $Ru^{4+}$ and $Ru^{4+}$ ions or $Ru^{4+}$and $Ru^{5+}$ ions [Figs. 7(a) and 7(c)] contain electrons also in higher-energy antibonding states. Actually, the number of dimers with the configuration $Ru^{5+}$-$Ru^{4+}$ accompanied by spin $S = 1/2$ must be quite small based on the observed small Curie constant.

The situation where most of the Ru ions form isovalent-spinless dimers is actually difficult to realize if $Ru^{5+}$ and $Ru^{4+}$ ions are distributed randomly. Thus, Ru ions in the D phase may exhibit charge ordering between $Ru^{4+}$ and $Ru^{5+}$ ions. This charge ordering may be the origin of the observed superlattice.

We now discuss the possible origin of the multiple magnetic transitions observed in the delithiated sample. As shown in Figs. 7(a) and 7(b), the MO $\delta^*$ is occupied by two electrons for a $Ru^{4+}$-$Ru^{4+}$ dimer, while this MO is empty for a $Ru^{5+}$-$Ru^{5+}$ dimer. Since the $\delta^*$ MO has a higher energy than the other occupied MOs, it is more likely that the MO $\delta^*$ of $Ru^{4+}$-$Ru^{4+}$ dimers breaks up at lower temperature than the others. As a consequence, the decomposition temperature of $Ru^{4+}$-$Ru^{4+}$ dimers is expected to be lower than that of $Ru^{5+}$-$Ru^{5+}$ dimers. Because electrons associated with decomposed dimers have active spins as shown in Fig. 7(d), dimer decomposition results in a higher magnetic susceptibility. Thus, similarly to the S phase, the enhancement of magnetization in the D phase above ~539 K (Sec. III B) is probably related to the breaking of MOs of $Ru^{4+}$-$Ru^{4+}$ dimers and enhancements at higher temperatures are related to $Ru^{5+}$-$Ru^{5+}$ dimers.

In the context of the linear combination of atomic orbitals, the bond lengths $L$ of different dimer configurations can be estimated in terms of the quantity called the bond order $B$, which is evaluated as

$$B = \tfrac{1}{2}(n_b - n_a), \tag{3}$$

where $n_b$ and $n_a$ are the numbers of electrons in the bonding and antibonding states, respectively. In Fig. 7 the values of $B$ of the possible electronic configurations are shown. Pauling found an empirical relation between $B$ and the bond length $L$ [31,32],

$$L = L_0 - f\log_{10}(B), \tag{4}$$

where the value of $f$ depends on the atoms and $L_0$ is the bond length for $B = 1$. Later this relation was derived from the Friedel model [33]. In order to evaluate the constant $f$, we use the value of the bond length of the dimer-liquid state of the S phase ($L_0 = 2.68$ Å) [12], where only the $\sigma$ MO is occupied, i.e., $B = 1$ [Fig. 7(d)]. We also use the bond lengths of the short bond in the dimer-solid state of the S phase ($L = 2.58$ Å), where the $\sigma$, $\pi$, $\delta$, and $\delta^*$ MOs are occupied, i.e., $B = 2$ [Fig. 7(a)]. From these values, we obtain $f = 0.332$ Å. Using these values we estimate the length of the $Ru^{5+}$-$Ru^{5+}$ bond in the dimer-solid state to be $L = 2.52$ Å.

Since in the dimer-solid state of the $x \approx 0.73$ sample, around 73% of the dimers are formed by $Ru^{5+}$-$Ru^{5+}$ ions and the rest by $Ru^{4+}$-$Ru^{4+}$ions, the average length of the short bonds is expected to be 2.56 Å if we assume that the dimers are all located in $L_2$ bonds. This is 0.04 Å shorter than the dimer entirely formed between $Ru^{4+}$and $Ru^{4+}$ ions in the S phase. On the other hand, the observations for the sum of the bond lengths ($L_T = L_1 + L_2 + L_3$) of the D phase ($L_T = 8.592$ Å) is 0.074 Å shorter than that of the S phase ($L_T = 8.666$ Å). The excess shrinkage of $L_T$ may be due to the difference in ionic size between $Ru^{4+}$ ($r = 0.62$ Å) and $Ru^{5+}$ ($r = 0.565$ Å) [34] in the nondimer bonds, although covalency needs to be considered. The reduced difference between short and long bonds in the D phase suggests that some dimers are distributed in $L_1$ and $L_3$ as well.

## IV. CONCLUSION

We have successfully synthesized delithiated-phase $Li_{2-x}RuO_3$, the D phase, with structures distinct from those of stoichiometric $Li_2RuO_3$, the S phase. For the first time, we identify the magnetic properties of the D phase. We find that Ru ions also form dimers as in the S phase. There should be two kinds of dimers in the D phase: $Ru^{4+}$-$Ru^{4+}$ dimers as in the S phase and additional $Ru^{5+}$-$Ru^{5+}$ dimers. The latter should have a new MO configuration, in which no electrons occupy

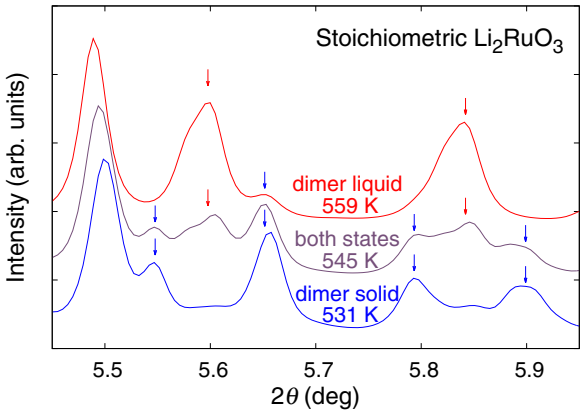


FIG. 8. High-energy XRD spectra of pristine $Li_2RuO_3$ sample at three temperatures: below $T_d \sim 550$ K, close to $T_d$, and above $T_d$ . It shows the coexistence of the dimer-solid and dimer-liquid states, which is typical of a first-order transition. Blue arrows indicate peaks characteristic of the dimer-solid state; red arrows, peaks of the dimer-liquid state. Measurements with $E = 87.5$ keV ($\lambda = 0.141$ Å) were performed at beam line ID11 of ESRF.

antibonding states. We find that above $T \approx 539$ K the D phase exhibits a strong increase in the susceptibility. In analogy to the S phase, this magnetic feature is most likely associated with the change from the dimer-solid to the dimer-liquid state. Structural and magnetic properties indicate that dimers in the dimer-solid state are located not only in $L_2$ bonds but also in $L_1$ and $L_3$ bonds. This dimer distribution may lead to the observed superlattice structure.

## ACKNOWLEDGMENTS

We thank G. Khaliullin, Z. Fisk, H. Takagi, M. Braden, and T. Fröhlich for useful discussions. We are grateful to Y. Honda for his support in the chemical composition analysis. We also acknowledge J. Wright and M. Di Michiel for their support. This work was supported by Grants-in-Aid for Scientific Research on Innovative Areas "Topological Materials Science" (JSPS KAKENHI Grant No. JP15H05852), as well as JSPS KAKENHI Grant No. JP26247060. M.-P.J.-S. was supported by a Japanese government (MEXT) scholarship.

## APPENDIX A: REACTION OF $Li_{2-x}RuO_3$ AT HIGH TEMPERATURES

In the XRD spectra shown in Fig. 4, the peak intensities of the $RuO_2$ ($P4_2/mnm$) peaks at 625 K are markedly higher than those at 583 K. See, for example, the peak at $2\theta = 2.57$. We find that this enhancement starts at ≈609 K (not shown in the figure). The structure of the main phase after heating above $T \approx 609$ K is equivalent to that of S-phase $Li_2RuO_3$.

Besides, as shown in Fig. 5 the temperature dependence of the susceptibility of $Li_{2-x}RuO_3$ $x \approx 0.73$ changes substantially before and after heating to 700 K. The behavior after heating to 700 K becomes similar to that of pristine $Li_2RuO_3$ (compare purple and black lines in Fig. 5). During further repeating of magnetization measurements of $x \approx 0.34$ and $x \approx 0.73$ samples, the obtained curves remain almost equivalent to the purple curve in Fig. 5.

These results indicate that, when $Li_{2-x}RuO_3$ is heated above $T \approx 609$ K, it decomposes into $Li_2RuO_3$ and $RuO_2$ according to the following reaction:

$$Li_{2-x}RuO_3 \xrightarrow[\text{air or He}]{\text{heat in}} \left(\frac{2-x}{2}\right)Li_2RuO_3 + \frac{x}{2}RuO_2 + \frac{x}{4}O_2. \quad \text{(A1)}$$

This decomposition reaction seems to be triggered by the loss of oxygen.

The minor phase $Li_{2-x}RuO_3$, with $x \approx 1.1$ (SG $R\bar{3}$), decomposes at lower temperatures. The peak at $2\theta = 1.75^\circ$, shown as a shoulder in Fig. 4, characteristic of this phase, disappears at 497 K. The magnetization exhibits a small change in slope at this temperature (Fig. 5).

## APPENDIX B: FIRST-ORDER TRANSITION OF THE S PHASE $Li_2RuO_3$

Initially the dimer transition of pristine $Li_2RuO_3$ was considered to be second order [9]. However, recent studies indicate that the dimer transition is a first-order transition [10,11]. Figure 8 shows the high-energy XRD spectra of pristine $Li_2RuO_3$ at three temperatures. At the temperature close to the dimer transition, the spectrum shows a combination of the structures of the dimer-solid and dimer-liquid states. This coexistence provides additional evidence for a first-order transition.

[1] Y. Singh and P. Gegenwart, Phys. Rev. B **82**, 064412 (2010).
[2] T. Takayama, A. Kato, R. Dinnebier, J. Nuss, H. Kono, L. S. I. Veiga, G. Fabbris, D. Haskel, and H. Takagi, Phys. Rev. Lett. **114**, 077202 (2015).
[3] A. Kitaev, Ann. Phys. **321**, 2 (2006).
[4] A. Shitade, H. Katsura, J. Kunes, X.-L. Qi, S.-C. Zhang, and N. Nagaosa, Phys. Rev. Lett. **102**, 256403 (2009).
[5] Y.-Z. You, I. Kimchi, and A. Vishwanath, Phys. Rev. B **86**, 085145 (2012).
[6] T. Hyart, A. R. Wright, G. Khaliullin, and B. Rosenow, Phys. Rev. B **85**, 140510 (2012).
[7] S. Okamoto, Phys. Rev. B **87**, 064508 (2013).
[8] D. D. Scherer, M. M. Scherer, G. Khaliullin, C. Honerkamp, and B. Rosenow, Phys. Rev. B **90**, 045135 (2014).
[9] Y. Miura, Y. Yasui, M. Sato, N. Igawa, and K. Kakurai, J. Phys. Soc. Jpn. **76**, 033705 (2007).
[10] M.-P. Jimenez-Segura, A. Ikeda, S. Yonezawa, and Y. Maeno, Phys. Rev. B **93**, 075133 (2016).
[11] I. Terasaki, S. Abe, Y. Yasui, R. Okazaki, and H. Taniguchi, J. Mater. Chem. C **3**, 10430 (2015).
[12] S. A. J. Kimber, I. I. Mazin, J. Shen, H. O. Jeschke, S. V. Streltsov, D. N. Argyriou, R. Valenti, and D. I. Khomskii, Phys. Rev. B **89**, 081408 (2014).

[13] S. Sarkar, P. Mahale, and S. Mitra, J. Electrochem. Soc. **161**, A934 (2014).
[14] H. Kobayashi, R. Kanno, Y. Kawamoto, M. Tabuchi, O. Nakamura, and M. Takano, Solid State Ion. **82**, 25 (1995).
[15] S. Taminato, M. Hirayama, K. Suzuki, K. Kim, Y. Zheng, K. Tamura, J. Mizuki, and R. Kanno, J. Mater. Chem. A **2**, 17875 (2014).
[16] D. Mori, H. Kobayashi, T. Okumura, and Y. Inaguma, Electrochemistry **83**, 1071 (2015).
[17] H. Kobayashi, R. Kanno, Y. Kawamoto, M. Tabuchi, and O. Nakamura, Solid State Ion. **86–88**, 859 (1996).
[18] M. Sathiya, G. Rousse, K. Ramesha, C. P. Laisa, H. Vezin, M. T. Sougrati, M.-L. Doublet, D. Foix, D. Gonbeau, W. Walker, A. S. Prakash, M. Ben Hassine, L. Dupont, and J.-M. Tarascon, Nat. Mater. **12**, 827 (2013).
[19] M. Sathiya, K. Ramesha, G. Rousse, D. Foix, D. Gonbeau, A. S. Prakash, M. L. Doublet, K. Hemalatha, and J.-M. Tarascon, Chem. Mater. **25**, 1121 (2013).
[20] B. Li, R. Shao, H. Yan, L. An, B. Zhang, H. Wei, J. Ma, D. Xia, and X. Han, Adv. Funct. Mater. **26**, 1306 (2016).
[21] D. C. Harris, *Quantitative Chemical Analysis*, 7th ed. (W. H. Freeman, San Francisco, 2006).
[22] P. Patnaik, *Dean's Analytical Chemistry Handbook*, 2nd ed. (McGraw–Hill Education, New York, 2004).
[23] J. S. Kouvel and M. E. Fisher, Phys. Rev. **136**, A1626 (1964).
[24] H. Lei, W.-G. Yin, Z. Zhong, and H. Hosono, Phys. Rev. B **89**, 020409 (2014).
[25] K. Momma and F. Izumi, J. Appl. Crystallogr. **44**, 1272 (2011).
[26] J. Park, T.-Y. Tan, D. T. Adroja, A. Daoud-Aladine, S. Choi, D.-Y. Cho, S.-H. Lee, J. Kim, H. Sim, T. Morioka, H. Nojiri, V. V. Krishnamurthy, P. Manuel, M. R. Lees, S. V. Streltsov, D. I. Khomskii, and J.-G. Park, Sci. Rep. **6**, 25238 (2016).
[27] G. A. Bain and J. F. Berry, J. Chem. Educ. **85**, 532 (2008).
[28] J. M. Fletcher, W. E. Gardner, B. F. Greenfield, M. J. Holdoway, and M. H. Rand, J. Chem. Soc. A**1968**, 653 (1968).
[29] S. Yonezawa, T. Higuchi, Y. Sugimoto, C. Sow, and Y. Maeno, Rev. Sci. Instrum. **86**, 093903 (2015).
[30] Y. Miura, M. Sato, Y. Yamakawa, T. Habaguchi, and Y. Ono, J. Phys. Soc. Jpn. **78**, 094706 (2009).
[31] L. Pauling, J. Am. Chem. Soc. **69**, 542 (1947).
[32] L. Pauling, Mineral. Soc. Am. Spec. Pap. **3**, 125 (1970).
[33] Adrian P. Sutton, *Electronic Structure Of Materials* (Oxford University Press, New York, 1993).
[34] R. D. Shannon, Acta Crystallogr. Sec. A **32**, 751 (1976).